Joint Pathology Center
Veterinary Pathology Services

WEDNESDAY SLIDE CONFERENCE 2022-2023

Conference #16 **18 January 2023**

CASE I:

Signalment:
11-year-old, intact male, snow leopard (*Panthera uncia*)

History:
The animal was diagnosed with COVID-19 via PCR and was doing well until an acute decline. Frank hemorrhage exuded from the nares, and blood was present on rectal.

Gross Pathology:
Gross Description: A moderate amount of dark red, dried blood was adhered to the fur around both nares. The thoracic cavity contained 164 mL of serosanguinous, semi-translucent fluid with few strands of fibrin. The lungs were red to dark red, wet, and edematous. Scattered throughout the lung were few tan to white mottled, nodular to multinodular masses, the largest of which was 4.0 cm x 3.2 cm x 2.7 cm. Similar nodules were present within the heart, bulging from the left atrioventricular endocardium and extending into the myocardium. The cortex and medulla of both kidneys were also expanded by numerous randomly scattered tan, bulging, masses like those within the lung and heart.

Laboratory Results:
1. Thoracic radiographs: Bilateral alveolar pattern of the caudodorsal lung fields
2. Covid-N rRT-PCR: Positive
3. In situ hybridization with v-SARS-CoV-2-N-01 (N gene) probe of lung, nasal, and tracheal sections: Distinct punctate staining in rare sloughed epithelial cells within nasal passages, in cells within alveoli (macrophages and/or sloughed epithelial cells), and within rare pneumocytes lining alveoli. These findings confirm the presence of SARS-CoV-2 RNA within tissue sections, albeit at low levels.

4.18s rRNA PCR Sequencing of FFPE Lung tissue: 99.70% identity to *Scedosporium apiospermum*

Microscopic Description:
Lung: Scattered throughout the lung parenchyma are multiple large nodules composed of a core of eosinophilic and karyorrhectic cell debris mixed with abundant fibrin, some edema, and hemorrhage. Cores are surrounded by a dense rim of numerous necrotic

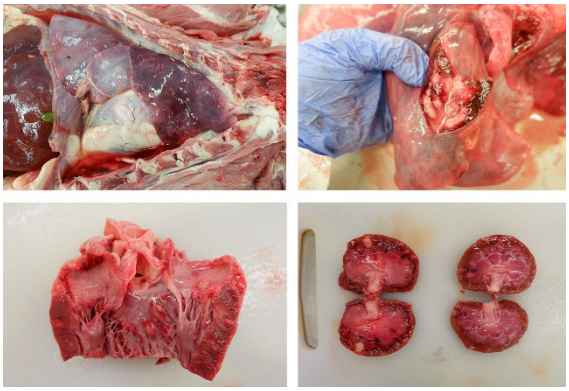

Figure 1-1. Multiple organs, snow leopard. White nodules are scattered throughout the lung, endocardium, and kidneys. (Photo courtesy of: (Photo courtesy of: University of Illinois at Urbana-Champaign, Veterinary Diagnostic Laboratory)

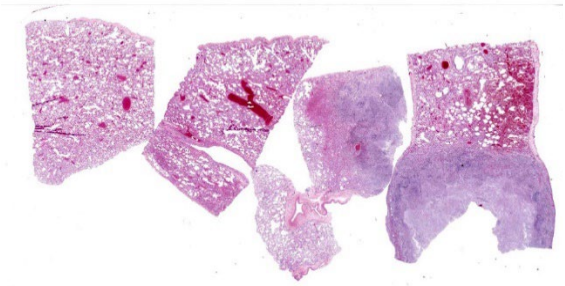

Figure 1-2. Lung, snow leopard. Two sections of lung (right) contain a large nodule of necrosis and inflammation which obscures pulmonary parenchyma. (HE, 7X)

neutrophils and epithelioid macrophages mixed with fewer lymphocytes and plasma cells. Throughout the necrotic cores and extending into the inflammatory rim are numerous fungal hyphae that are 3-6 µm wide with parallel walls, regular septations, dichotomous acute angle branching, and bulbous dilatations (presumptive ascomycete fungus). Throughout these nodules, septal vessels often contain thrombi composed of layers of lamellated fibrin. In many areas, septa are coagulatively necrotic, characterized by maintained architecture with diffuse hypereosinophilic and loss of nuclear detail. Rarely, necrotic debris is mineralized. Many alveolar septa are expanded by congestion, eosinophilic fibrillar material (fibrin), clear and colorless space (edema) and foamy macrophages; some septa contain smooth muscle hypertrophy and hyperplasia. Type 1 pneumocytes are often absent and replaced by deeply eosinophilic lamellar material (hyaline membranes). In some areas type 1 pneumocytes are replaced by cuboidal epithelium which segmentally lines alveolar spaces (type 2 pneumocyte hyperplasia). Alveolar spaces are frequently filled with variable combinations of foamy macrophages, eosinophilic proteinaceous material (edema), extravasated erythrocytes, fibrin, and neutrophils. Similar accumulations are present in many bronchioles and bronchi.

Other histopathology findings that are not included in the provided slide:

- Multifocal, chronic, pyogranulomatous necrotizing encephalitis, myocarditis, nephritis, and bilateral retinitis and choroiditis, with left eye scleritis and posterior uveitis, with intralesional hyphae
- Moderate, diffuse, chronic rhinitis with fibrosis
- Moderate, multifocal to coalescing, lymphoplasmacytic tracheitis with erosions and ulcerations

Contributor's Morphologic Diagnoses:

1. Lung: Marked, subacute interstitial pneumonia with type-2 pneumocyte hyperplasia and hyalin membrane formation, and marked hemorrhage and edema
2. Lung: Marked, multifocal, chronic, pyogranulomatous necrotizing pneumonia with intralesional hyphae.

Contributor's Comment:

Two main processes are identified in this animal, which contributed to death. The first is significant alveolar damage and interstitial inflammation accompanied by abundant pulmonary edema and hemorrhage, which is histologically compatible with SARS-CoV2 infection. The pathophysiologic mechanisms of COVID-19 are incompletely understood, however direct effects are primarily limited to the lung, while systemic disease occurs via

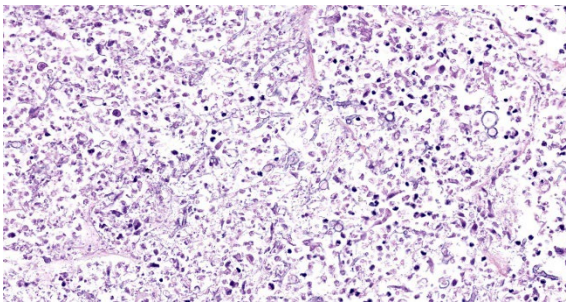

Figure 1-3. Lung, snow leopard. Within the area of necrosis, there are numerous 4-6 µm septate dichotomously branching fungal hyphae with bulbous swelling. (HE, 381X)

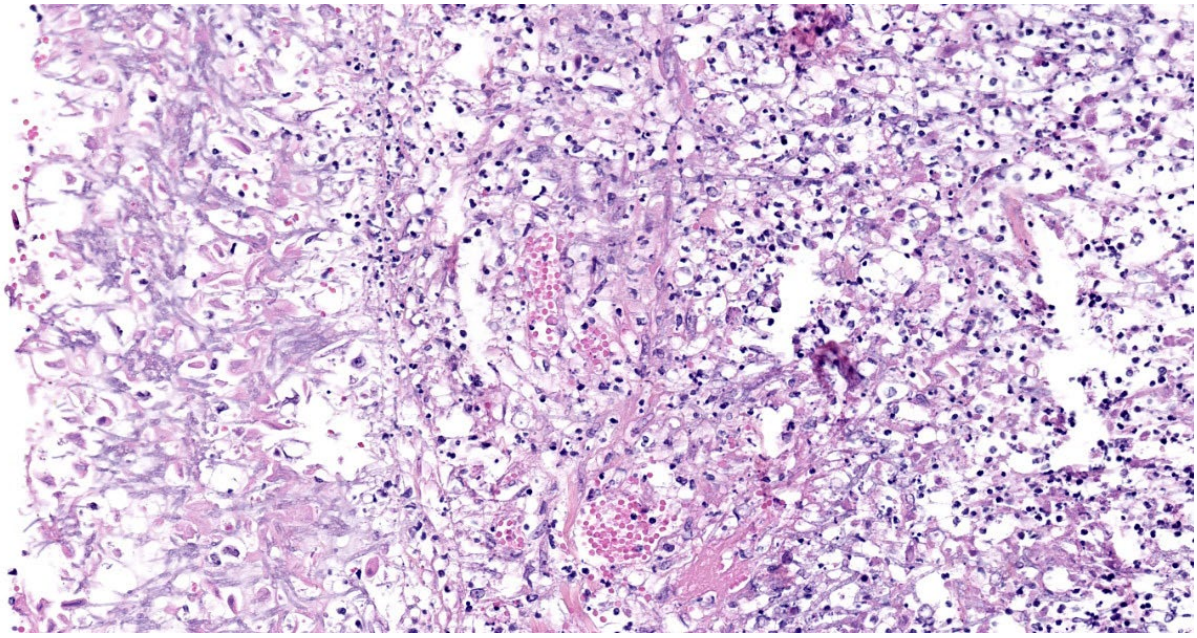

Figure 1-4. Lung, snow leopard. A large mat of fungal hyphae expands the pleura and extends into the pleural space (at left). (HE, 265X)

secondary effects.[2] Within humans, the histopathologic lesions associated with severe COVID-19 are consistent with Diffuse Alveolar Damage (DAD) secondary to Acute Respiratory Distress Syndrome (ARDS). DAD is not specific for COVID-19, and can be induced by various causes, including mechanical ventilation, various pulmonary infections, thermal injury, toxic gas exposure, and septicemia.[3]

The exact appearance of DAD will vary depending on the chronicity. An acute, exudative phase occurs during the first week after pulmonary injury, and is characterized by congested alveolar septa, and alveoli filled with copious protein-rich edema and fibrin. Inflammation is generally low unless DAD is the result of previous pneumonia. The formation of hyalin membranes—aggregates of fibrin, other serum proteins, and cell debris which line alveoli and alveolar ducts, impeding the junction between the airspace and the septum—is an important characteristic histologic finding.[3,10] Over time, DAD will progress into an organizing or proliferative phase, characterized by interstitial proliferation of fibroblasts and myofibroblasts, accompanied by type 2 pneumocyte hyperplasia and squamous metaplasia.[2] Microvascular thrombi are also frequently seen with COVID-19, however it is speculated that this lesion is more associated with ARDS than COVID-19 specifically.[2]

COVID-19 has been seen within multiple animal species, including domestic cats, domestic dogs, tigers, lions, gorillas and snow leopards (USDA Confirmed Cases of SARS-CoV-2 in animals in the United States). A recent study has shown that domestic cats (*Felis catus*) can be utilized as an infection model for COVID-19, displaying similar clinical and histopathologic as in humans.[13] COVID-19 viral infection and replication within a host depends on the presence and distribution of angiotensin-converting enzyme 2 (ACE2) receptors.[2] The ACE2 receptor within cats is similar in structure and distribution to humans, which may contribute to the similarities in clinical and histologic findings.[13] It has not been studied if these same principles apply to large felids such as snow

leopards. Within this case, interstitial and alveolar changes within the lung are consistent with a sub-acute DAD response transitioning between the exudative phase and proliferative phase. While there are multiple differentials for a DAD response within this animal, in situ hybridization confirms COVID-19 infection within the epithelial cells of the nasal passages and rare pneumocytes of the alveoli.

The second process in this case consists of severe pyogranulomatous and necrotizing lesions throughout multiple organs, including the lung, brain, heart, kidneys, and the choroid and retina of both eyes. Sequencing of the fungal organisms within these lesions identifies it as *Scedosporium apiospermum*, an opportunistic filamentous fungus found worldwide.[6] Once considered the asexual form of *Pseudoallescheria boydii,* recent taxonomic changes upon introduction of molecular phylogenetics places *S. apiospermum* within the *Scedosporium* genus, where it is the most pathogenic of the included species.[4,14] *S. apiospermum* is of increasing importance in human medicine, where it can cause severe systemic infections within immunocompromised and immunocompetent patients. Rare cases of both localized and disseminated infections have been reported in various animal species, including the dog, cat, horse, and a stranded northern elephant seal.[1,4,8,9]

Diagnosis of a *Scedosporium* infection is difficult due to clinical and histopathologic similarities to *Aspergillus, Fusarium,* and other hyalin hyphomycetes.[7] Subtle histologic differences between *Scedosporium* and *Aspergillus* do exist, including slightly more irregular branching within *Scedosporium* vs the more regular and dichotomous branching pattern of *Aspergillus*. Additionally, *Scedosporium* will commonly have terminal or intercalary, globose chlamydospores, thick-walled structures up to 20um in diameter which can be confused with yeasts.[7] These differences are subtle, and further testing such as in situ hybridization, culture, or molecular sequencing are important for definitive diagnosis. It is likely that *Scedosporium* is underdiagnosed in veterinary medicine due

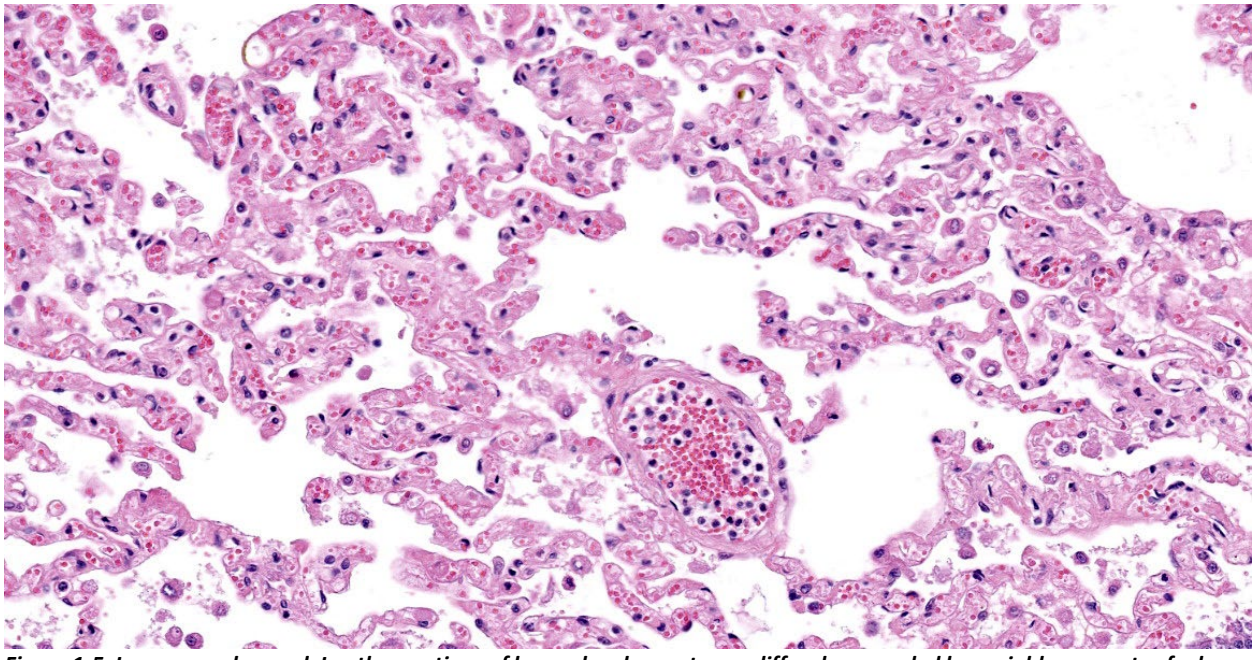

Figure 1-5. Lung, snow leopard. In other sections of lung, alveolar septa are diffusely expanded by variable amounts of edema, congestion, fibrin, and few Type II pneumocytes. There is mild alveolar edema and low numbers of alveolar macrophages (HE, 251X)

to its similarities to other fungal species.[4] Definitive diagnosis of *Scedosporium* is important, due to differences in antifungal resistance profile from *Aspergillus*.[6]

In this case, it is speculated that the primary COVID-19 infection led to immunocompromise of the animal, and systemic opportunistic infection by *Scedosporium apiospermum*, demonstrating both the importance of COVID-19 within the snow leopard species, and the growing importance of *Scedosporium apiospermum* within veterinary medicine.

Contributing Institution:
University of Illinois at Urbana-Champaign, Veterinary Diagnostic Laboratory

JPC Diagnosis:
1. Lung: Pneumonia, interstitial, necrotizing, subacute, diffuse, marked, with septal thrombosis, hemorrhage, and type II pneumocyte hyperplasia.
2. Lung: Pleuropneumonia, pyogranulomatous and necrotizing, multifocal, severe, with innumerable fungal hyphae.

JPC Comment:
A review of recent literature demonstrates that experimental severe acute respiratory syndrome coronavirus 2 (SARS-CoV2) infection in domestic cats can produce a spectrum of clinical disease and histologic lesions. As the contributor describes, one possible outcome is diffuse alveolar damage, as described by Rudd et al in a 2021 *Viruses* article.[13] In Rudd's study, the virus was inoculated directly into the trachea of 12 nine-month-old specific pathogen free (SPF) cats; six cats were used as controls.[13] Inoculated cats developed clinical signs of illness, including lethargy, fever, and dyspnea, and histologic evidence of diffuse alveolar damage.[13]

In a prior study, Gaudreault et al inoculated 6 five-month-old SPF cats with a slightly larger volume of the same strain of virus, but through nasal and oral routes.[5] These animals remained asymptomatic but transmitted the virus to co-housed, uninfected animals.[5] Histopathologic findings were minimal to moderate and localized to conducting airways, with lymphocytic and neutrophilic inflammation of the tracheobronchial seromucous glands which resolved by 21 days post challenge.[5]

Finally, a more recent study published by Patania et al in *Vet Pathol* described a different pattern of interstitial pneumonia with occlusive bronchiolitis in experimentally infected cats.[12] Ten SPF cats, ages 19 to 24 week, were inoculated by a different viral strain through intraocular, intranasal, tracheal, and oral routes.[12] No control cats were used. The cats remained asymptomatic, but on histology, there was patchy interstitial pneumonia, histiocytic bronchiolitis, and persistent interstitial thickening. Most of the cats lacked diffuse alveolar damage.[12] Bronchiolar lumens were often occluded by adherent plugs of epithelioid macrophages.[12] Early in the disease, interstitial and alveolar septal thickening was partially attributed to a mixed inflammatory infiltrate composed of B lymphocytes, T lymphocytes, and macrophages.[12] Once the inflammation resolved, interstitial thickening persisted and was attributed to endothelial hyperplasia, proliferative and disorganized capillaries, and individualized type II pneumocyte hyperplasia only appreciable with cytokeratin IHC; fibrosis was not a feature in thickened septae.[12] One of the three cats evaluated at 28 days post-challenge had more severe changes, including atelectasis, vasculitis, and inflammatory exudates and fibrin within alveoli.[12]

The differences in the results of these studies illustrate the wide range of lesions which may

be induced by experimental SARS-CoV2 infections in cats, and differences in study design (routes of inoculation, challenge dose, viral strain used) and individual host responses may account for these results.

Invasive fungal diseases (IFD) secondary to SARS-CoV-2 infection occur with relative frequency in hospitalized human patients.[11] Up to 7.6% of hospitalized COVID-19 experience pulmonary aspergillosis due to *Apsergillus fumigatus*, and this coinfection has a mortality rate of 56%.[11] Other documented coinfections include candidiaisis and mucormycosis, most commonly due to *Rhizopus.*[11] There are multiple possible reasons why COVID-19 patients are more susceptible to fungal infections, including tissue damage, immune dysfunction, and individual host factors or preexisting conditions. Viral infection impairs mucocilliary clearance and causes local tissue damage, exposing hidden host receptors permissive to fungal invasion.[11] Viral induced lymphopenia, depletion and dysfunction of dendritic cells, and local hypoxia attenuate the immune response to fungal invasion; this can be exacerbated by the use of immunsuppressive agents prescribed for controlling the overwhelming inflammatory response.[11] Chronic viral infection leads to decreased numbers of CD8+ T cells and NK cells, and remaining cells may demonstrate an ineffective and immune-exhausted phenotype (expressing PD1 and NKG2A, respectively) which create risk factors for IFB.[11] COVID-19 may also cause impaired fungicidal activity by neutrophils, leading to impaired innate immunity.[11]

References:

1. Berzina I, Trumble NS, Novicki T, et al. Subconjunctival mycetoma caused by *Scedosporium apiospermum* infection in a horse. *Vet Clin Pathol*. 2011; 40(1):84-88.
2. Caramashi S, Kapp ME, Miller SE, et al. Histopathological findings and clinicopathologic correlation in COVID-19: a systematic review. *Mod. Pathol.* 2021; 34:1614-1633.
3. Caswell JL, Williams KJ. Respiratory System. In: Maxie MG, ed. *Jubb, Kennedy, and Palmer's Pathology of Domestic Animals.* Vol 2. 6th ed. St. Louis, MO: Elsevier; 2016.
4. Di Teodoro G, Averaimo D, Primavera Miria, et al. Disseminated *Scedosporium apiospermum* infection in a Maremmano-Abruzzese sheepdog. *BMC Vet Res*. 2020: 16(2):372.
5. Gaudreault NN, Trujillo JD, Carossino M. SARS-CoV-2 infection, disease and transmission in domestic cats. *Emerg Microbes Infect*. 2020; 9(1): 2322-2332.
6. Goldman C, Akiyama MJ, Torres J, et al. *Scedosporium apiospermum* infections and the role of combination therapy and GM-CSF: A case report and review of the literature. *Med. Mycol Case Rep.* 2016; 11:40-43.
7. Guarro J, Kantarcioglu AS, Horre R, et al. *Scedosporium apiospermum*: a changing clinical spectrum of a therapy-refractory opportunist. *Med. Mycol*. 2006; 44(4):295-327.
8. Haulena M, Buckles E, Gulland FMD, et al. Systemic mycosis caused by *Scedosporium apiospermum* in a stranded northern elephant seal (*Mirounga angustirostris*) undergoing rehabilitation. *J. Zoo Wildl Med. 2002;* 33(2):166-171.
9. Leperlier D, Vallefuoco R, Laloy E, et al. Fungal rhinosinusitis caused by *Scedosporium apiospermum* in a cat. *J Feline Med Surg*. 2010; 12:697-971.
10. Montero-Fernandez MA, Pardo-Garcia R. Histopathology features of the lung in COVID-19 patients. *Diagn Histopathol*. 2021; 27(3):123-127.

11. Morton CO, Griffiths JS, Loeffler J, Orr S, White PL. Defective antifungal immunity in patients with COVID-19. *Front Immunol.* 2022; 13:1-11.
12. Patania OM, Chiba S, Halfmann PJ, et al. Pulmonary lesions induced by SARS-CoV-2 infection in domestic cats. *Vet Pathol*. 2022; 59(4): 696-706.
13. Rudd JM, Selvan MT, Cowan S, et al. Clinical and histopathologic features of a feline SARS-CoV-2 infection model are analogous to acute COVID-19 in humans. *Viruses.* 2021;13(8):1550.
14. Taylor A, Talbot J, Bennett P, et al. Disseminated *Scedosporium prolificans* infection in a Labrador retriever with immune mediated haemolytic anaemia. *Med Mycol Case Rep*. 2014; 6:66-69.

CASE II:

Signalment:
Juvenile, male intact, bobcat (*Lynx rufus*)

History:
The bobcat presented to a wildlife rehabilitation center for right hind lameness, dehydration, and emaciation. The bobcat initially improved with therapy but after a couple of weeks of hospitalization deteriorated rapidly and died.

Gross Pathology:
The spleen was slightly enlarged with a meaty consistency and had multifocal, sparse, pinpoint, white foci throughout the parenchyma. The retropharyngeal, mesenteric and renal lymph nodes were moderately to markedly enlarged and on the cut surface had many white to pale tan foci. The liver was brown and had multifocal, pinpoint to 0.1 cm white foci throughout the parenchyma. The right distal tibia was slightly expanded by a bony proliferation (interpreted as callus). The abdominal cavity contained approximately 40 ml of yellow, transparent, viscous to slightly gelatinous fluid.

Laboratory Results:
Immunohistochemistry:
Feline coronavirus antigen specific immunohistochemistry performed on the section of ileum was negative.

Bacteriology:
Francisella tularensis was isolated from the liver by aerobic culture.

Molecular diagnostics:
The isolated bacteria were confirmed to be *Francisella tularensis* type A based on PCR.

Microscopic Description:
Ileum – Multifocally, Peyer's patches are largely effaced by variably-sized, central areas of eosinophilic cellular and basophilic karyorrhectic debris admixed with degenerate neutrophils (lytic necrosis) which are surrounded by moderate to large numbers of epithelioid macrophages. Multifocally infiltrating the surrounding submucosa are moderate numbers of lymphocytes, plasma cells, neutrophils and macrophages. The outer longitudinal lamina muscularis is multifocally effaced by small areas of lytic necrosis and cellular debris, and within the inner circular lamina muscularis there are multifocal, often perivascular clusters of lymphocytes, plasma

Figure 2-1. Multiple organs, bobcat. A selection of organs is submitted on this individual. The tissue of interest is a section of ileum with attached lymph node (right). (HE, 6X)

cells, neutrophils and macrophages. The attached mesentery is multifocally effaced by large areas of lytic necrosis as well as moderate numbers of lymphocytes, plasma cells and macrophages with fewer neutrophils, admixed with fibrillar, brightly eosinophilic material (fibrin). Within the mucosa there is a reduced density of crypts, with widespread blunting of villi and expansion of the lamina propria with moderate numbers of neutrophils and fewer lymphocytes, plasma cells and macrophages. Within the superficial mucosa and intestinal lumen are multifocal small colonies of mixed bacteria, as well as moderate numbers of apicomplexan coccidian organisms in various developmental stages, including: few schizonts containing numerous basophilic, elongate merozoites; numerous uninucleate, eosinophilic macrogametes; numerous oocysts containing pale eosinophilic granular material; and rare large microgamonts with numerous condensed, basophilic nuclei.

Mesenteric lymph node – The mesenteric lymph node associated with the ileum is markedly expanded and almost completely effaced by a large, central area of lytic necrosis as previously described, admixed with macrophages, neutrophils, and fibrin. Few small to moderately sized aggregates of mature lymphocytes and plasma cells remain scattered throughout the section.

Contributor's Morphologic Diagnoses:
1. Ileum:
a. Ileitis, pyogranulomatous and necrotizing, multifocal, severe, chronic.
b. Intraepithelial coccidian organisms, moderate.

2. Mesenteric lymph node, lymphadenitis, pyogranulomatous and necrotizing, widespread, severe, chronic.

Contributor's Comment:
Francisella tularensis, the causative agent of tularemia, is a gram negative, obligate aerobe, intracellular coccobacillus of the gamma-subclass of Proteobacteria.[10,12] There are currently 4 recognized subspecies: subspecies *tularensis* (type A), which is highly

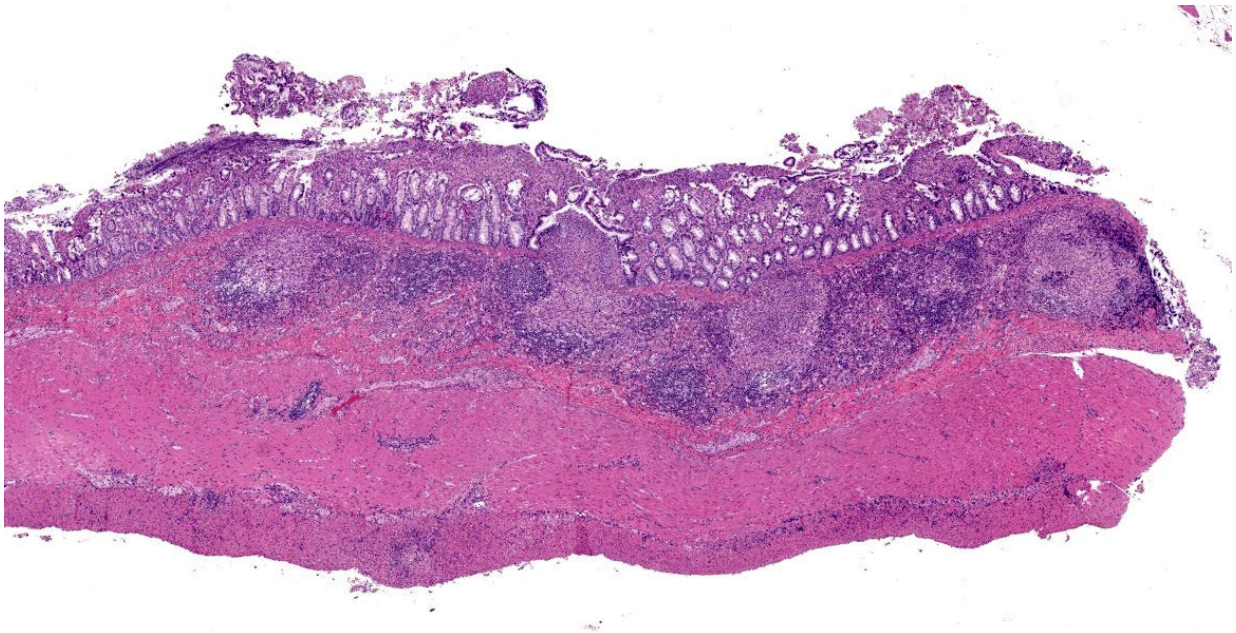

Figure 2-2. Ileum, bobcat. There are changes in all layers of the wall. There is ulceration of the mucosa and marked cellular infiltration of the underlying lamina propria. There is marked necrosis of the submucosal Peyer's patches. There is necrotizing vasculitis and lymphangitis of the muscularis and serosa. (HE, 32X)

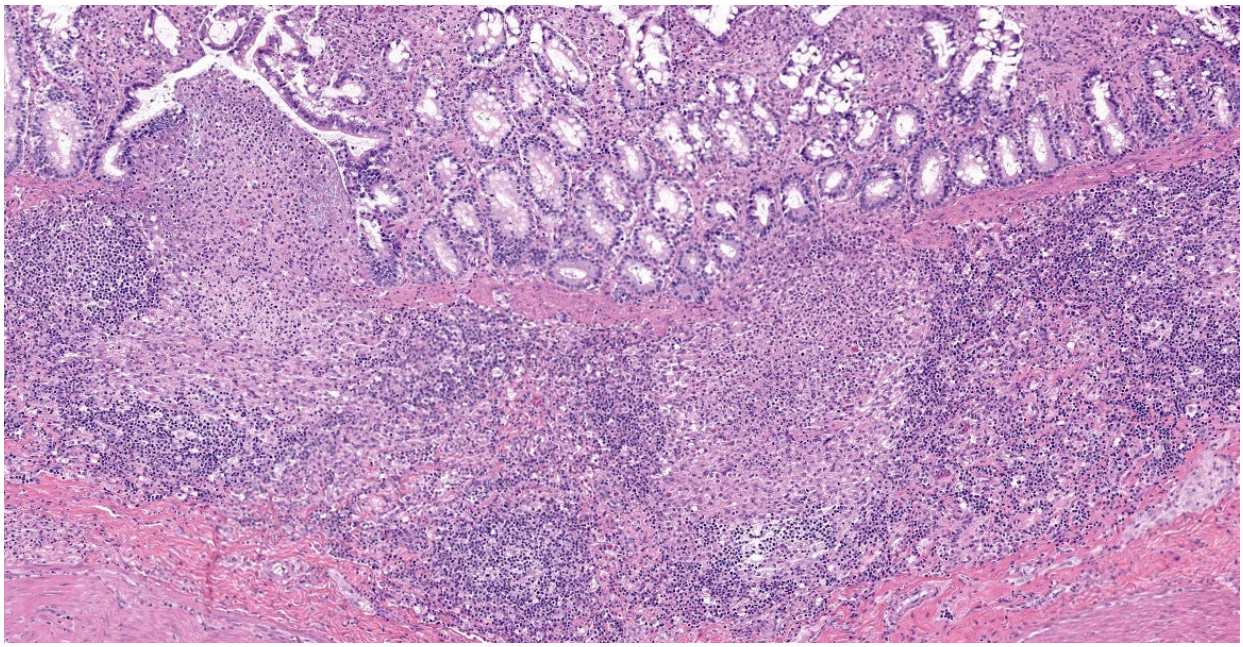

Figure 2-3. Ileum, bobcat. There is marked lymphoid depletion and focal necrosis within the ileal Peyer's patch) (HE, 88X)

virulent in domestic animals and humans, predominantly found in North America, and is most commonly associated with lagomorphs; subspecies *holarctica* (type B), which is less virulent, endemic throughout the Northern Hemisphere, and more frequently associated with rodents and waterborne disease; subspecies *novicida*, which is mostly avirulent in humans and predominantly found in North America; and subspecies *mediasiatica*, which is also considered to be avirulent in humans and predominantly found in Russia and central Asia.[11] The type A subspecies is further divided into 2 distinct subpopulations, A1 and A2. In the USA, A1 subpopulations occur primarily in the eastern half of the country while A2 subpopulations occur primarily in the west.[9]

F. tularensis has a wide and varied range of hosts, with a list of known susceptible species including 190 mammals, 88 invertebrates, 23 birds and 3 amphibians, with occasional reports in reptile and fish species.[6] Although lagomorphs and rodents are frequently implicated in the spread and maintenance of this disease, there has been no evidence to suggest that they act as a major reservoir.[7,12] Transmission to humans can occur via a number of different routes, including handling of infected animals, ingestion of improperly cooked infected meat or contaminated water, inhalation of infective aerosols, and arthropod bites.[9] Important arthropod vectors for transmitting *F. tularensis* in the USA include hard ticks, deer flies, stable flies and horseflies. Of those, hard ticks are considered to be the primary vectors for type A strains; ticks of the *Ambylomma* and *Dermacentor* genera are typically responsible for human cases while ticks of the *Ixodes* and *Haemophysallis* genera are more important in maintaining enzootic foci among wildlife.[4,9] Sheep are historically considered to be the domestic mammal most commonly associated with tularemia type A, however, in the past few decades domestic cats have become an increasing source for zoonotic transmission.[4]

Gross lesions in affected animals typically involve miliary white foci within the spleen, liver and lymph nodes, as well as splenomegaly, hepatomegaly and lymphadenopathy.[8] These lesions are grossly indistinguishable from the lesions caused by *Yersinia* species. Histologically, these white foci are composed

of multifocal areas of lytic necrosis, admixed with degenerate neutrophils and/or surrounded by macrophages and fibroblasts in older lesions. *F. tularensis* bacteria are generally difficult to visualize histologically in routine H&E and even Gram-stained sections, whereas *Yersinia* species bacteria tend to be readily visible.

In this bobcat, there was a translucent, straw colored, viscous, serofibrinous abdominal effusion, reminiscent of the effusion which characterizes the wet form of feline infectious peritonitis (FIP). In the submitter's experience, this is an atypical finding for tularemia. Therefore, and because bacteria were not detected within the lesions, immunohistochemistry for feline coronavirus antigen was performed on the section of ileum; however, coronaviral antigen was not detected within any of the cells in the section.

The coccidian organisms within the lumen of this bobcat's ileum were morphologically most similar to *Cystoisospora felis*. In a recent paper, *C. felis*-like organisms were found in feces of 2 bobcats and transmitted to domestic cats.[2] Unlike *C. felis* in domestic cats which develops within the villar epithelium, the schizonts and gamonts of these *C. felis*-like coccidia were located within the lamina propria of the ileum, indicating that they are likely to be a similar but different parasite to *C. felis* of domestic cats. In our

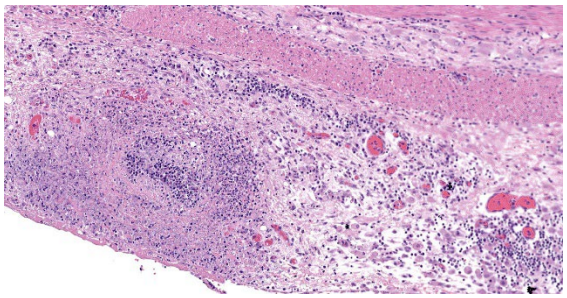

Figure 2-4. Ileum, bobcat. There is necrotizing vasculitis and diffuse inflammation and edema within the serosa. (HE, 173X)

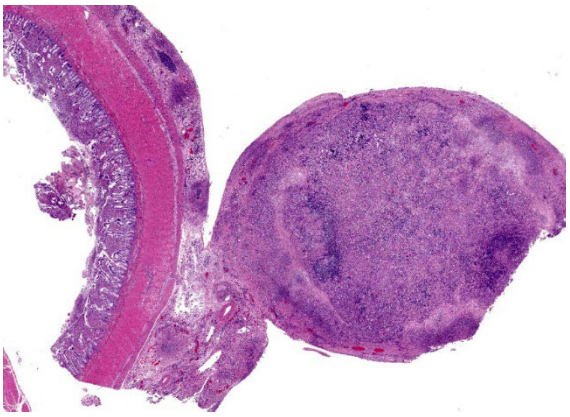

Figure 2-5. Mesenteric lymph node, bobcat. There is diffuse necrosis and loss of nodal architecture. (HE, 15X)

bobcat's case, it is difficult to assess the organisms' location with certainty due to the significant blunting and disruption of the villi. In addition, the significance of the mixed colonies of bacteria within the intestinal lumen is unknown. While they may have contributed to the suppurative ileitis, it is also possible that they represent an intraluminal 'bystander' population.

F. tularensis is a tier 1 agent on the US Department of Health and Human services biological select agents list as it has the potential to pose a severe threat to public health and safety.[3] As a consequence of being on this list, there are strict regulations involved when handling *F. tularensis*. The agent and all tissues that contain the agent must be destroyed, and this destruction must be reported. Appropriate personal protective equipment (PPE) should be worn when this agent is suspected, including gloves and a cut-resistant glove, an impermeable apron, lab boots, a face shield, and a respirator such as a properly fitted N95 mask.

Contributing Institution:
Veterinary Diagnostic Laboratory, University of Minnesota, St Paul, MN.
https://vdl.umn.edu/

JPC Diagnosis:
1. Ileum: Ileitis, necrotizing, diffuse, moderate, with multifocal vasculitis and Peyer's patch necrosis.
2. Mesenteric lymph node: Lymphadenitis, necrotizing, diffuse, severe.
3. Mesentery, vessels: Vasculitis, necrotizing, severe.
4. Ileum: Coccidial gamonts and oocysts, multiple.
5. Pancreas and adipose tissue: Zymogen granule depletion and fat atrophy.

JPC Comment:
During the conference, the participants and moderator, COL(R) Derron (Tony) Alves, remarked on the marked vasculitis along the serosa and within the mesentery and prominent reactive mesothelium suggestive of abdominal effusion. Before knowing the clinical history and laboratory results, participants considered the possibility of FIP based on these histologic lesions, but the contributor ruled this out using immunohistochemical staining. Participants also had spirited discussion regarding inflammation surrounding areas of lymphoid necrosis in Peyer's patches and lymph nodes; some felt this would qualify as pyogranulomatous inflammation, while others felt that the remaining cells represented residual dendritic cells associated with lymphoid follicles.

In 1909, a researcher investigating bubonic plague in squirrels in California discovered a novel bacterium which caused enlarged lymph nodes.[5] The bacteria was dubbed *Bacterium tularense*, reflecting where it was discovered – Tulare county. This new bacterium was not directly contagious but could be transmitted via infected blood, tissue, or fleas. [5] The first confirmed infection in a human occurred in a butcher in Ohio in 1911. [5] In the early 1920s, researchers in Montana conducting wood tick surveillance for Rocky Mountain Spotted Fever discovered that

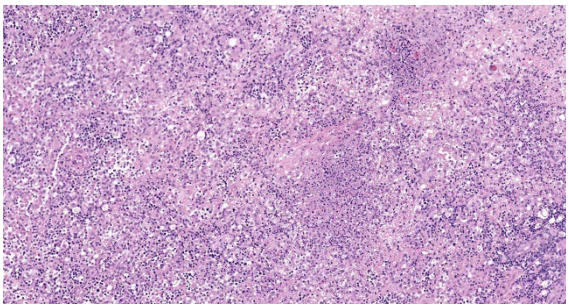

Figure 2-6. Mesenteric lymph node, bobcat. There is marked lymphoid depletion, tingible body macrophages, and multifocal areas of lytic necrosis within the submitted node. (HE, 125X)

some ticks were infected with *B. tularense* and could pass this infection to animals. [5] Furthermore, these ticks could transmit the bacterium transovarially and would remain infected for life. [5]

Around the same time, Edward Francis began his research in Utah on "Deer Fly Fever", a condition in humans caused by *B. tularense* featuring fever, lymphadenitis, and draining tracts from affected nodes.[5] In 1928, Francis published a thorough report on 629 human cases of *B. tularense*, and the bacterium was later renamed *Francisella tularense* in acknowledgement of his extensive research.[5] This rechristening was also fitting in that Francis was frequently affected by the disease himself: he was infected at least five times during his life, likely due to his reluctance to wear gloves during autopsies.[5]

Of the cases reported by Francis, 400 were attributed to contact with rabbits, and 70 were attributed to tick bites.[5] The disease had an incubation period of less than 10 days and resulted in acute fever with two to three months of convalescence.[5] The most common clinical presentation was the ulceroglandular form, as an ulcer formed at the site of exposure and regional lymphadenitis resulted in a draining tract over the inflamed "gland".[5] Other reported forms included oculoglandular (where conjunctival exposure resulted in

conjunctivitis, corneal ulceration, and regional lymphadenitis), glandular form (similar to ulceroglandular form without cutaneous lesions), and typhoidal (systemic disease lacking ocular, cutaneous, and lymph node involvement).[5] Additional forms subsequently described include an oropharyngeal form and pneumonia.[5]

F. tularensis is a facultative intracellular parasite which can survive and replicate in a variety of host cells, including macrophages, dendritic cells, neutrophils, endothelial cells, type II pneumocytes, and hepatocytes.[1] The pathogencity of *Francisella* is associated with intracytoplasmic replication within macrophages.[13] The bacteria induces phagocytosis by binding to mannose receptors; the C3 complement receptor, scavenger receptor A, nucleolin, or lung surfactant protein A once opsonized; or the Fcγ receptor once antibody-opsonized.[1] The microbe survives within the phagosome by delaying phagosome maturation, inhibiting NADPH oxidase activation, and resisting the effects of reactive oxygen species.[1,13] While other bacteria which live in the cytosol use lipid hydrolases or phospholipases to escape the phagosome (such as *Listeria*), *Francisella* is unique in that it likely uses a type VI secretion system for phagosome egress.[1,13] The bacterium then uses "nutritional virulence" to adapt to the cytosolic environment.[13] *Francisella* LPS has low endotoxicity and is not recognized by TLR4; rather, the bacteria triggers TLR2 signaling, activates both the AIM-2 and NLRP3 inflammasomes, and ultimately results in production of proinflammatory cytokines IL1 beta and pro-IL8.[1] Apoptosis or pyroptosis of infected cells leads to liberation of the bacteria, which can then infect new cells.[1,13] The bacteria can also directly penetrate adjacent cells using trogocytosis.[13]

References:

1. Celli J, Zahrt TC. Mechanisms of *Francisella tularensis* Intracellular Pathogenesis. *Cold Spring Harb Perspect Med*. 2013; v.3(4):1-14.
2. Dubey JP, Houk AE, Verma SK, Calero-Bernal R, Humphreys JG, Lindsay DS. Experimental transmission of C*ystoisospora felis*-like coccidium from bobcat (*Lynx rufus*) to the domestic cat (*Felis catus*). *Vet Parasitol*. 2015;211(1-2):35-39.
3. Federal Select Agent Program, US Department of Health and Human Services, accessed May 31, 2022. <https://www.selectagents.gov/>
4. Friend M. *Tularemia*. Circular 1297. U.S. Geological Survey; 2006
5. Hirschmann JV. From Squirrels to Biological Weapons: The Early History of Tularemia. *Am J Med Sci.* 2018; 356(4): 319-328.
6. Keim P, Johansson A, Wagner DM. Molecular epidemiology, evolution, and ecology of *Francisella*. *Ann N Y Acad Sci*. 2007;1105:30-66.
7. Lamps LW, Havens JM, Anders S, Page DL, Scott MA. Histologic and molecular diagnosis of tularemia: a potential bioterrorism agent endemic to North America. *Mod Pathol.* 2004;17:489-495.
8. Maxie MG, Jubb KVF, Kennedy PC, Palmer N. *Jubb, Kennedy, and Palmer's Pathology of Domestic Animals*. Elsevier Saunders; 2007.
9. Petersen JM, Mead PS, Schriefer ME. *Francisella tularensis*: an arthropod-borne pathogen. *Vet Res*. 2009;40(2):7.
10. Quinn PJ, Markey BK, Leonard FC, Fitz-Patrick ES, Fanning S, Hartigan PJ. *Veterinary Microbiology and Microbial Disease*. John Wiley & Sons; 2011.
11. Timofeev V, Titareva G, Bahtejeva I, et al. The comparative virulence of *Francisella tularensis* subsp. *mediasiatica* for vaccinated laboratory animals. *Microorganisms*. 2020;8(9):1403.

12. World Health Organization. *WHO Guidelines on Tularemia*. WHO Press; 2007.
13. Ziveri J, Barel M, Charbit A. Importance of Metabolic Adaptations in *Francisella* Pathogenesis. *Front Cell Infect Microbiol*. 2017; 7(96): 1-8.

CASE III:

Signalment:
2-month-old male entire Domestic Shorthair (*Felis catus)*

History:
A two-month-old kitten owned for 10 days with a history of diarrhoea and vomiting for the past 24 hours, presented with hypoglycaemia and agonal breathing. Arrested, cardiopulmonary resuscitation performed for 20 minutes, and owner consented for cessation.

Gross Pathology:
At postmortem examination, the lungs are mottled pale pink to dark red, spongy, with a bullous appearance to all distal margins (marginal emphysema) and have variably pale pink, approximately 0.8 cm wide linear discolouration (rib impressions, presumed related to CPR noted in history). The stomach contains a small amount of pale brown-green, pasty ingesta. The orad small intestines contain moderate amounts of thin, yellow fluid that transitions to pale cream digesta within the jejunum and scant cream-yellow digesta within the ileum. The colon contains pale brown, flocculent, variably mucoid, and watery faeces, and pale brown pasty faeces are within the rectum. The mesenteric lymph node is enlarged (4.0 x 1.2 x 0.3 cm, within normal limits for a kitten), and the ileocecal and colonic lymph nodes are similarly prominent.

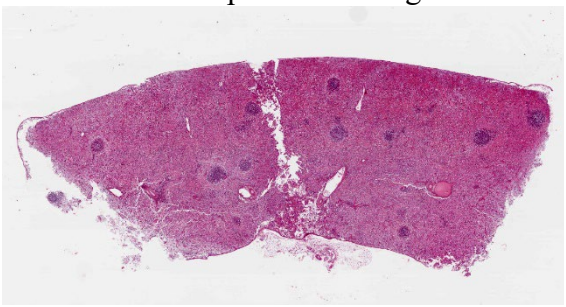

Figure 3-1. Spleen, cat. A section of markedly congested spleen is submitted for examination. White pulp is diffusely and markedly depleted and lacks mantle formation. (HE, 6X)

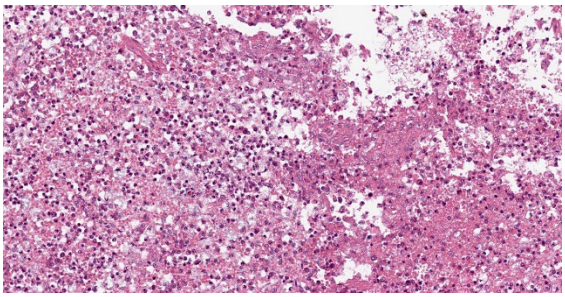

Figure 3-2. Spleen, cat. Scattered throughout the white matter are areas of lytic necrosis. (HE, 240X)

Additional findings included: reduced subcutaneous adipose tissue stores, pale pink oral mucous membranes, a prominent (age-appropriate) thymus, heart measurements within normal ratio, mild lobular pattern on the liver, moderately distended gall bladder, kidney measurements within normal limits, congested meninges, and pale skeletal muscle.

No significant gross abnormalities are detected in the following tissues: sciatic nerve, coxofemoral joints, femur bone, femur bone marrow, thyroid gland, parathyroid glands, tongue, pharynx, larynx, great cardiac vessels, adrenal glands, ureters, eyes, and ears.

Laboratory Results:
Faecal PCR Panel: Negative (below assay detection limits) for the following organisms: *Campylobacter, Salmonella, Giardia duodenalis, Cryptosporidium [C. parvum, C. hominis], Tritrichomonas foetus, Toxoplasma gondii, Dientamoeba fragilis, Neospora*

caninum, *Clostridium perfringens* enterotoxin cpe, Parvovirus, Distemper virus, Feline and Canine Coronavirus.

Faecal flotation: (Saturated sodium chloride, specific gravity 1.2): No evidence of eggs from nematodes or coccidia in the sample provided.

Microbiology: (spleen and liver): Samples of spleen and liver (collected at necropsy and frozen back for ancillary diagnostics if needed) were submitted for aerobic bacterial and fungal culture following initial histopathology review. After 24 hours incubation, cultures of both tissues yielded a pure heavy growth of a large, mucoid, lactose fermenting, non-haemolytic, gram-negative rod with colony morphology that was circular, raised, mucoid, smooth, grey, and approximately 3 mm diameter in size. The IMViC and urease profile for the isolates were as follows: Indole negative, Methyl Red negative, Voges-Proskauer positive, Citrate positive, Urease positive. Microbiology comments: The biochemical profile and colony morphology of the isolates are consistent with *Klebsiella pneumoniae* subsp. *pneumoniae*, and isolate identification has been confirmed by bioMérieux API20E assay.

Microscopic Description:
Spleen: White pulp follicles are smaller than expected and are widely separated by a hypercellular red pulp composed of erythrocytes interspersed with abundant homogenous eosinophilic material (presumed lysed erythrocytes), many macrophages and neutrophils, and myriad extracellular and intrahistiocytic bacterial rods, and scattered cellular debris and haematopoietic precursors. Additionally, throughout the sections, there are regionally extensive aggregates of approximately 2-4 microns round to ovoid discrete faintly eosinophilic structures with central round to elongate internal structures somewhat reminiscent of nuclei; Giemsa and Gram-stained replicate sections reveal a similar staining pattern to the marked proliferations of bacteria elsewhere throughout the parenchyma (suggestive of 'encapsulated' bacteria).

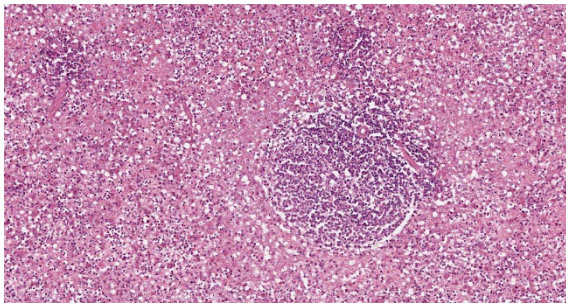

Figure 3-3. Spleen, cat. White pulp is severely depleted. (HE, 116X)

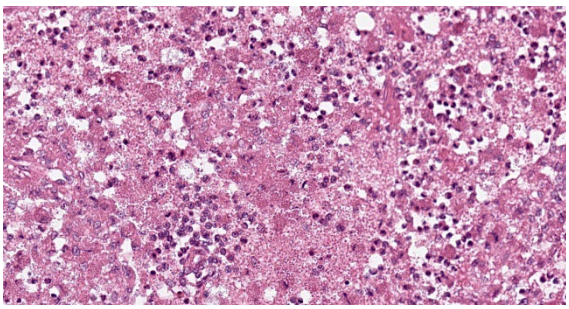

Figure 3-4. Spleen, cat. Throughout the white pulp, there are innumerable encapsulated bacilli which are also present in the cytoplasm of macrophages. (HE, 400X)

Contributor's Morphologic Diagnoses:
Splenitis, diffuse, histiocytic, and neutrophilic, acute to subacute, severe, with myriad extracellular and intrahistiocytic bacteria

Contributor's Comment:
Morbidity and mortality were ascribed to fulminant *Klebsiella pneumoniae* subsp. *pneumoniae* (Kpp) septicaemia and complications which most likely included multiple organ dysfunction syndrome (MODS) and systemic inflammatory response syndrome (SIRS). Numerous encapsulated Gram-negative rods were evident histologically within the vasculature of all evaluated tissues and within the parenchyma of blood filtering organs. While

some of this may be reflective of post-mortem overgrowth, the relatively short post-mortem interval combined with the identification of intracellular bacteria and acute inflammation in many tissues and heavy growth of pure cultures of Kpp isolated from spleen and lung support a diagnosis of severe antemortem bacteraemia. Kpp is an opportunistic bacterium found in the environment and as a commensal in the nasopharynx and alimentary tract of dogs and cats. Kpp can be associated with clinically significant infections of the respiratory, gastrointestinal and genitourinary tracts and systemic bacteraemia in carnivores. In some instances, underlying immunosuppression appears to have played a role in disease development (e.g., drugs, malnutrition, stress, endocrine disease, and other infections, including feline leukaemia virus, feline immunodeficiency virus infection). Kpp-induced enteritis, pneumonia, and sepsis with concurrent MODS has been reported in dogs. The diarrhoea and enteritis in this kitten were presumably related. Pneumonia was of sufficient severity to have resulted in some degree of respiratory compromise which was likely further exacerbated by SIRS, accounting for the clinically noted respiratory distress. In the medical and veterinary microbiology literature, the most common pathogenic bacteria that have capsules linked to virulence include are *Klebsiella pneumoniae, Escherichia coli, Haemophilus influenzae, Streptococcus pneumoniae, Yersinia pestis* and *Bacillus antracis,* where only the first four are gram-negative.[6]

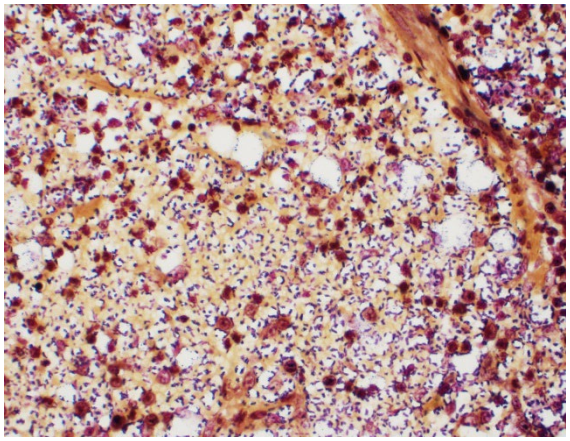

Figure 3-5. Spleen, cat. A gram stain demonstrates the widely spaced encapsulated bacilli characteristic of Klebsiella pneumoniae. (Brown-Brenn, 400X)

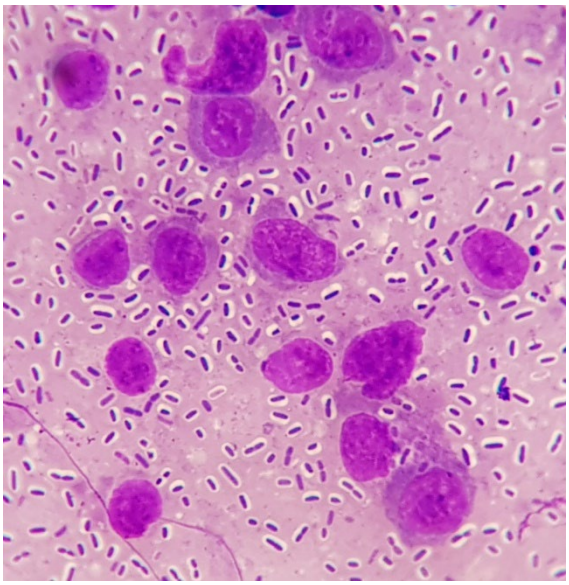

Figure 3-6. Spleen, cat. A rapid Diff-Quik stain on splenic cytology also demonstrates the encapsulated bacilli at the autopsy table. (Diff-Quik, 400X) (Photo courtesy of University of Sydney, https://sydney.edu.au/science/schools/sydney-school-of-veterinary-science/veterinary-science-services.html)

Contributing Institution:
University of Sydney
https://sydney.edu.au/science/schools/sydney-school-of-veterinary-science/veterinary-science-services.html

JPC Diagnosis:
Spleen: Splenitis, histiocytic and neutrophilic, diffuse, severe with lymphoid depletion, congestion, and innumerable extracellular and intrahistiocytic bacilli.

JPC Comment:
Klebsiella pneumoniae is associated with community-acquired, opportunistic, and nosocomial infections in both humans and animals and is one of the leading causes of healthcare-associated infections in humans. There are a wide range of virulence factors which contribute to its pathogenicity. Kpp has 78 distinct capsular serotypes, but K1 and

K2 are the most commonly isolated.[3,4] Its capsule prevents phagocytosis, blocks opsonization, and prevents complement-mediated lysis.[3] To acquire necessary iron, Kpp produces several sidephores, including enterobactin, yersiniabactin, salmochelin, and aerobactin.[3] Adhesins and type 1 and 3 fimbriae facilitate adhesion, invasion, and biofilm formation. Biofilms form on indwelling devices (such as catheters) and facilitate colonization of the gastrointestinal, respiratory, and urinary tracts.[3] Kpp utilizes quorum sensing to coordinate gene expression at certain bacterial densities.[3] Additionally, a hypervirulent strain of *K. pneumoniae* (hvKp) has emerged and is associated with serious community-acquired infections in humans, causing pneumonia, hepatic abscesses, meningoencephalitis, and septic arthritis.[3,4] This strain produces excess capsular material, causing hypermucosity, and higher quantities of siderophores than the classic strains.[3]

K. pneumoniae naturally produces chromosomal penicillinases, conferring resistance to ampicillin, carbenicillin, and ticarcillin; in the past four decades, however, *K. pneumoniae* has also collected additional antibiotic resistance plasmids, expanding its antibiotic resistance repertoire. Some strains are now developing resistance to carbapenem, previously considered a first-line treatment for this infection.[3]

A recent retrospective study of infections in 697 domestic animals in Brazil provides a glimpse of the spectrum of diseases caused by *K. pneumoniae.*[4] The urinary system was the most common system affected in dogs and cats, accounting for 51.9% of 393 canine cases and 63% of 27 feline cases; the infection caused cystitis, pyelonephritis, and urethritis in these species.[4] In cattle, 59.7% of 149 cases were due to mastitis; the majority of these were clinical and considered moderate to severe.[4] In 53.1% of 98 cases in horses, the bacteria was associated with reproductive infection, causing seminal vesiculitis, pyometra, abortion, and orchitis. In pigs, 59.1% of 22 cases were associated with diarrhea.[4]

References:

1. Green CE, Sykes J. *Infectious Diseases of the Dog and Cat.* 4th ed. St. Louis, MO: Elsevier Saunders; 2011:187-188.
2. Koenig A. Gram-Negative Bacterial Infections. In: Green CE, ed. *Infectious Diseases of the Dog and Cat.* 4th ed. St. Louis, MO: Elsevier. 2012: 353-355.
3. Piperaki ET, Syrogiannopoulos GA, Tsouvelekis LS, Daikos GL. *Klebsiella pneumoniae*: Virulence, Biofilm and Antimicrobial Resistance. *The Pediatric Infectious Disease Journal.* 2017; 36(10): 1002-1005.
4. Ribiero MG, de Morais ABC, Alves AC. *Klebsiella*-induced infections in domestic species: a case-series study in 697 animals (1997-2019). *Brazilian Journal of Microbiology*. 2022; 53: 455-464.
5. Roberts DE, McClain, HM, Hansen, DS, Currin P, Howerth, EW. An outbreak of Klebsiella pneumoniae infection in dogs with severe enteritis and septicemia. *J Vet Diagn Invest.* 2000; 12:168-173.
6. Tortora GJ, Funke BR, Case CL. *Microbiology: An Introduction.* 9th ed. San Francisco, CA: Pearson Benjamin Cummings.

CASE IV:

Signalment:
A 23.5-year-old female African green monkey (*Chlorocebus aethiops sabaeus*).

History:
This monkey had a three-year history gradual weight loss and a slow growing cranial abdominal mass.

Gross Pathology:
A 12x8x7 cm mottled tan to red soft multilobular mass extended from the wall of the greater curvature of the body of the stomach into the peritoneum. The omentum was firmly adhered to the mass and the adjacent small intestines, stomach, liver, and left kidney. On sectioned surface, the mass was mottled tan to red with large red to black areas of necrosis.

Laboratory Results:
No laboratory results reported.

Microscopic Description:
A well demarcated, partially encapsulated multilobular mass, expanding the muscularis externa and serosa, is composed of streams and bundles of closely spaced neoplastic mesenchymal cells supported by a fine fibrovascular stroma, and infiltrated by a few small aggregates of lymphocytes. The neoplastic cells range from 30x10-50x15 µm, have indistinct cell borders, abundant fibrillar to clear eosinophilic cytoplasm, and central oval to fusiform 10x10 -25x12 µm nuclei with finely stippled chromatin, without nucleoli. Mitoses occur at 0-1 per 10, 40x fields. Macrophages with intracytoplasmic golden-tan pigment (hemosiderin) infiltrate the capsule of the neoplasm. The overlying gastric mucosa is disorganized, thickened up to twice normal, with loss of polarity in the gastric pits and glands. Many of the gastric glands are lined by or have prominent parietal cells, and mitoses are numerous. Small hemorrhages are scattered throughout the lamina propria, and lymphoid aggregates along the deep mucosa are prominent. Few lymphocytes, eosinophils, and neutrophils infiltrate the muscularis mucosa. The smooth muscle of the tunica media of some arterioles in the submucosa are thickened, and the lumina are reduced in size. The neoplastic cells were immunohistochemically negative for smooth muscle actin (SMA) and positive for CD117.

Figure 4-1. Stomach, African green monkey. A 12x8x7 cm mottled tan to red multilobular mass extended from the wall of the greater curvature of the body of the stomach into the peritoneum. (Photo courtesy of: Wake Forest School of Medicine. Department of Pathology, Section on Comparative Medicine, Medical Center Boulevard, Winston-Salem, NC 27157, www.wakehealth.edu)

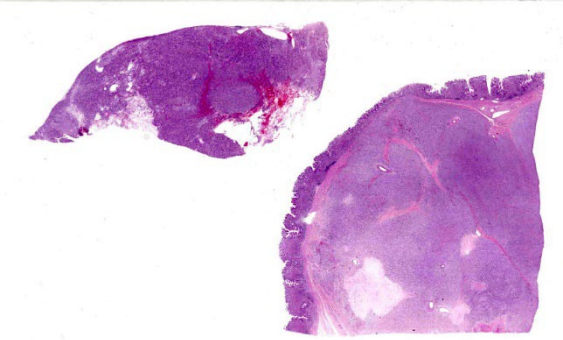

Figure 4-2. Stomach, African green monkey. Two sections of stomach are submitted for examination. In the larger section (with mucosa), the gastric wall is markedly distended by a mesenchymal neoplasm. (HE, 4X)

Transmission electron microscopy findings: The elongate neoplastic cells have medium electron-dense to electron lucent cytoplasm with few mitochondria, and fusiform euchromatic nuclei, some with single nucleoli. A few cells have two nuclei. The cells are separated by extracellular matrix containing 20

Table 4.1

Differential Diagnoses	Positive Immunohistochemical Stains
Leiomyoma	Smooth muscle actin (SMA)
Leiomyosarcoma	SMA
Peripheral nerve sheath tumor	CD99 / S100
Schwannoma	S100
Neurofibroma	S100 / CD34+ (focal)

nm wide electron-dense fibrils, electron lucent spaces, and amorphous medium electron dense-material.

Contributor's Morphologic Diagnoses:
Gastric body: Gastrointestinal stromal tumor

Contributor's Comment:
Gastrointestinal stromal tumors (GISTs) are rare mesenchymal tumors of the gastrointestinal tract which are thought to originate from the interstitial cells of Cajal. They have been reported in rhesus macaques, chimpanzees, baboons, and spider monkeys, numerous domestic animals, and humans.[1,2,3,10,13,14] In companion animals they most frequently arise in the intestine, whereas in humans and non-human primates, they primarily occur in the gastric cardia and body.[1,2,13]

Characteristic histologic findings include a herringbone pattern of mesenchymal cell proliferation supported by dense fibrovascular stroma, and in larger tumors necrosis is common. These tumors typically arise from the mucosa or submucosa, and transmural invasion is common.[10] The majority of GISTs are CD117 (c-KIT), CD34, and DOG-1 (discovered on gastrointestinal stromal tumors protein-1) positive.[13]

The majority of GISTs contain a mutation in the *KIT* receptor tyrosine kinase gene, resulting in the overexpression of the KIT protein, which can be identified immunohistochemi-

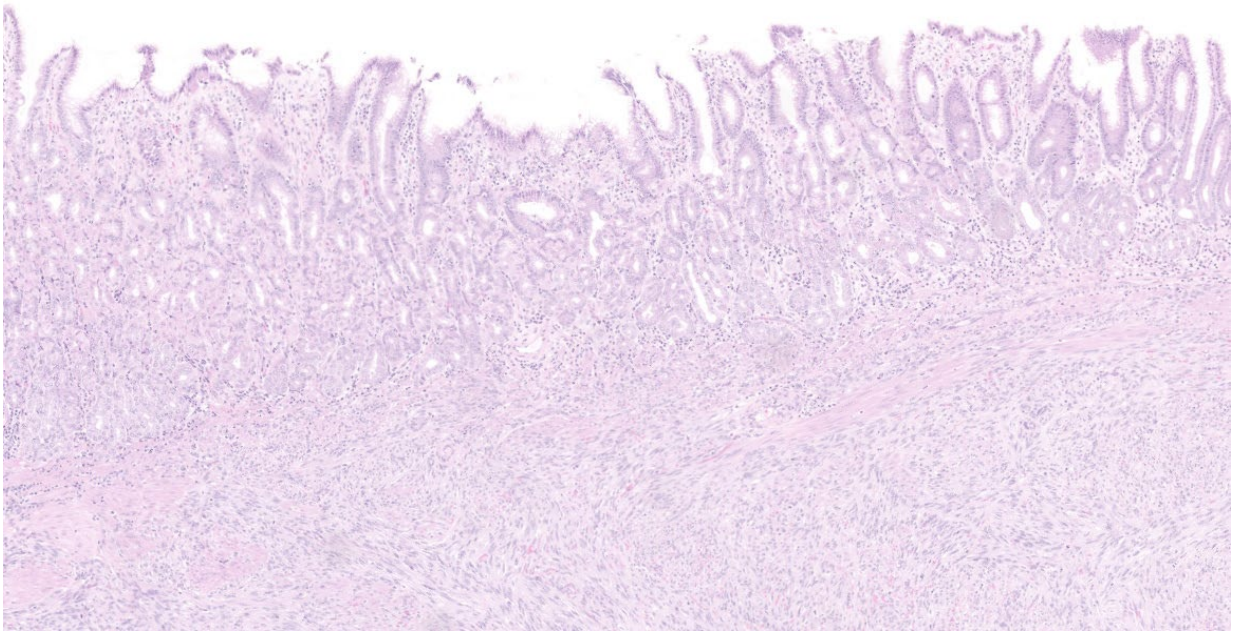

Figure 4-3. Stomach, African green monkey. A spindle cell neoplasm arises from the submucosa, effacing the wall and infiltrating the overlying mucosa. (HE, 73X)

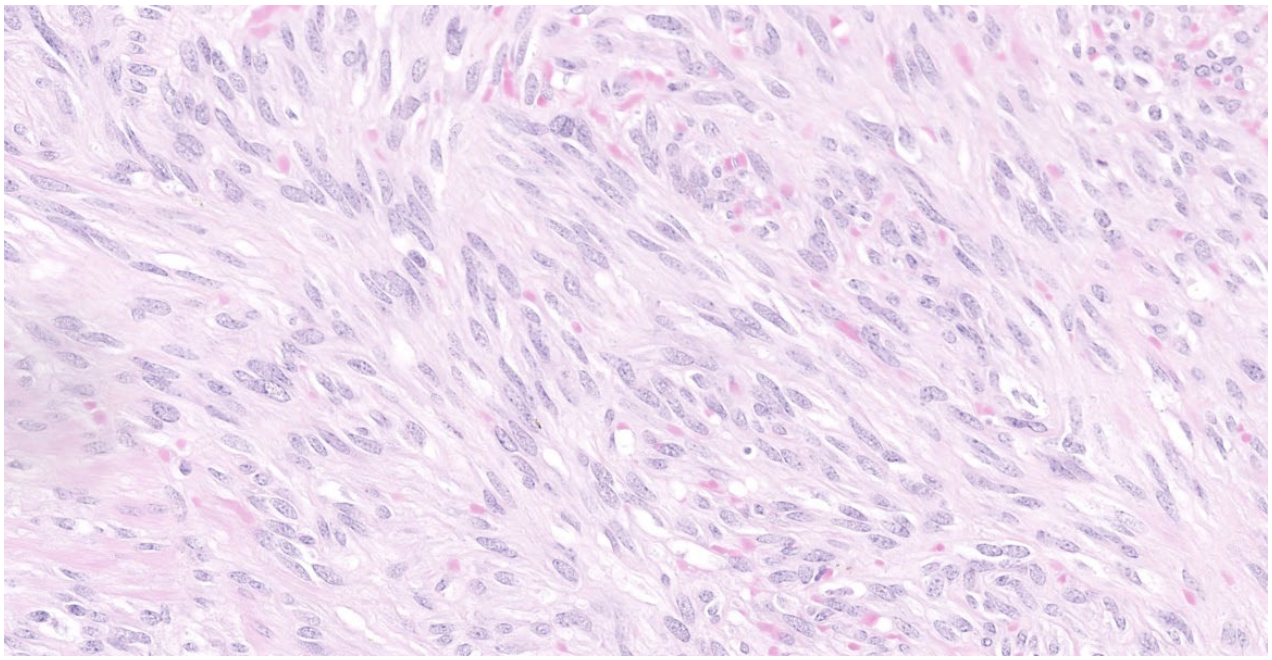

Figure 4-4. Stomach, African green monkey. High magnification of neoplastic cells. (HE, 73X)

cally with CD117 (c-KIT).[12] CD34, an antigen for hematopoietic progenitor and endothelial cells is positive in some interstitial cells of Cajal and in the majority of GISTs in humans and other species.[4,15] In humans and dogs, DOG-1 is a more sensitive and specific marker for GISTs than CD117. DOG-1 is independent of mutations in CD117, and has been documented to stain CD117- and CD34-negative GISTs.[5,8]

Ultrastructurally, GISTs are composed of primitive mesenchymal cells which may have non-membrane-bound electron lucent regions in the cytoplasm. Dense bodies, which are characteristic of smooth muscle, are present in leiomyomas and leiomyosarcomas, and absent in GISTs.[6] Some GISTs, particularly in the intestinal tract and rectum in humans, may have skeinoid fibers, of which the composition is unknown. Histologically they appear as extracellular hyaline globules. Ultrastructurally, skeinoid fibers are composed of medium electron-dense fibrils resembling collagen but with a periodicity of ~43 nm.[11,14] Skeinoid fibers were not identified in this case.

GISTs should be differentiated from leiomyomas, leiomyosarcomas, peripheral nerve sheath tumors, schwannomas, and neurofibromas because of the differences in metastatic potential and prognoses (Table 4.1). In humans, GISTs often arise in the gastric cardia and body, whereas leiomyomas are more common in the esophagus.[9,17]

Contributing Institution:
Wake Forest School of Medicine
Department of Pathology, Section on Comparative Medicine

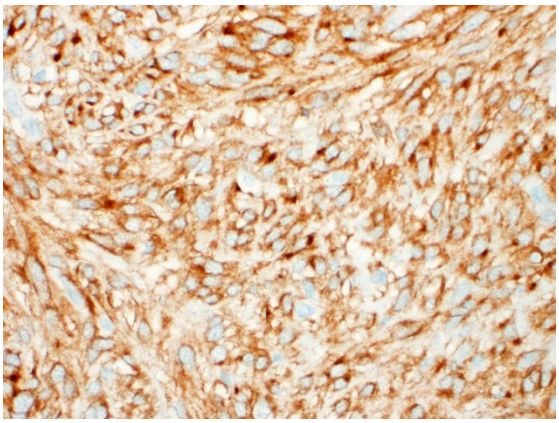

Figure 4-5. Stomach, African green monkey. Neoplastic cells are strongly positive for c-Kit. (anti-C-Kit, 400X)

Medical Center Boulevard, Winston-Salem, NC 27157
www.wakehealth.edu

JPC Diagnosis:
Stomach: Gastrointestinal stromal tumor.

JPC Comment:
As the contributor mentions, one of the differentials for gastrointestinal stromal tumors (GISTs) is a smooth muscle neoplasm, such as leiomyoma and leiomyosarcoma.[7] Historically, human GISTs humans were diagnosed as smooth muscle neoplasms prior to ultrastructural evaluation and the discovery of the CKIT protooncogene marker of these neoplasms.[7] Leiomyomas and leiomyosarcomas have historically been the most common spindle cell neoplasm of the gastrointestinal tract in rats and mice in the National Toxicology Program's two-year bioassays, so researchers recently conducted a retrospective study evaluating CKIT expression in smooth muscle tumors of these species.[7] In B6C3F1/N mice, 22 of 32 tumors (69%) previously diagnosed as leiomyoma/leiomyosarcoma were CKIT positive, indicating they are likely GISTs.[7] Most (16) of these tumors arose in the cecum, with fewer in the colon and stomach. In rats, all of the tumors were negative for CKIT, and most were positive for desmin and smooth muscle actin, confirming their diagnosis as smooth muscle tumors.[7] These surprising results indicate that GISTs are more common than leiomyoma/leiomyosarcomas in mice in the NTP bioassays.[7]

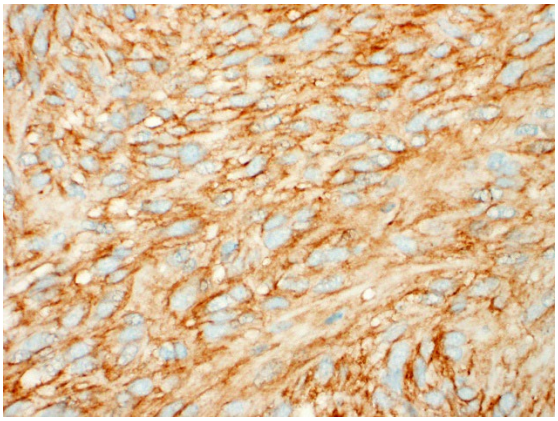

Figure 4-6. Stomach, African green monkey. Neoplastic cells are strongly positive for DOG-1. (anti-DOG-1, 400X)

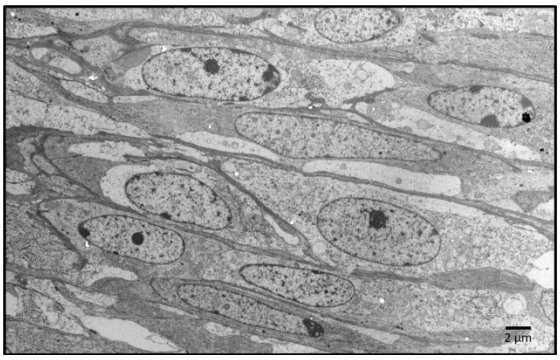

Figure 4-7. Stomach, African green monkey. Transmission electron micrograph of the neoplastic cells. The cells have regions of electron lucency and lack the dense bodies typical for smooth muscle. (Photo courtesy of: Wake Forest School of Medicine. Department of Pathology, Section on Comparative Medicine, Medical Center Boulevard, Winston-Salem, NC 27157, www.wakehealth.edu)

Another recent study described gastrointestinal stromal tumors (GISTs) in four guinea pigs of advanced age.[16] Three animals had neoplasms in the gastric wall at the cardia, while the fourth was in the small intestine.[16] One of the gastric GISTs metastasized to the duodenal and cecal mesentery.[16] The gastric GISTs were positive for c-KIT, DOG-1, and smooth muscle actin.[16] The small intestinal GIST was negative for smooth muscle actin, but positive for c-KIT and DOG-1.[16] In all neoplasms, atypia was mild and mitotic figures were rare. Additionally, all cases had deletion mutations in exon 11 of the *Kit* gene.[16]

References:

1. Banerjee M, Lowenstine LJ, Munn RJ. Gastric stromal tumors in two rhesus macaques (*Macaca mulatta*). *Vet Pathol*. 1991; 28: 30-36.
2. Bommineni YR, Dick EJ, Jr., Hubbard GB. Gastrointestinal stromal tumors in a baboon, a spider monkey, and a chimpanzee and a review of the literature. *J Med Primatol*. 2009; 38: 199-203.

3. Brown SL, Anderson DC, Dick EJ, Jr., Guardado-Mendoza R, Garcia AP, Hubbard GB. Neoplasia in the chimpanzee (*Pan* spp.). *J Med Primatol*. 2009; 38: 137-144.
4. Bure I, Braun A, Kayser C et al. The expression of hematopoietic progenitor cell antigen CD34 is regulated by DNA methylation in a site-dependent manner in gastrointestinal stromal tumours. International Journal of Cancer 141: 2296-2304, 2017
5. Dailey DD, Ehrhart EJ, Duval DL, Bass T, Powers BE. DOG1 is a sensitive and specific immunohistochemical marker for diagnosis of canine gastrointestinal stromal tumors. *J Vet Diagn Invest*. 2015; 27: 268-277.
6. Ferenczy A, Richart R, Okagaki T. A comparative ultrastructural study of leiomyosarcoma, cellular leiomyoma, and leiomyoma of the uterus. *Cancer.* 1971; 28: 1004-1018.
7. Janardhan KS, Venkannagari P, Jensen H, et al. Do GISTs Occur in Rats and Mice? Immunohistochemical Characterization of Gastrointestinal Tumors diagnosed as Smooth Muscle Tumors in the National Toxicology Program. *Toxicol Pathol.* 2019; 47(5):577-584.
8. Jung JH, Im S, Choi HJ, Lee YS, Jung ES. Gastrointestinal stromal tumor with dedifferentiation to undifferentiated pleomorphic sarcoma. *Pathol Int*. 2013; 63: 479-482.
9. Levy AD, Remotti HE, Thompson WM, Sobin LH, Miettinen M. Gastrointestinal stromal tumors: radiologic features with pathologic correlation. *Radiographics*. 2003; 23: 283-304, 456; quiz 532.
10. Meuten DJ. *Tumors in Domestic Animals*. Fifth edition. Ames, IO: Wiley Blackwell. 2017.
11. Min KW: Gastrointestinal stromal tumor: an ultrastructural investigation on regional differences with considerations on their histogenesis. *Ultrastruct Pathol.* 2010; 34: 174-188.
12. Novelli M, Rossi S, Rodriguez-Justo M, Taniere P et al. DOG1 and CD117 are the antibodies of choice in the diagnosis of gastrointestinal stromal tumours. *Histopathology*. 2010; 57: 259-270.
13. Parab TM, DeRogatis MJ, Boaz AM, et al. Gastrointestinal stromal tumors: a comprehensive review. *J Gastrointest Oncol*. 2019; 10: 144-154.
14. Saito T, Ueno M, Ota Y et al. Histopathological and clinical characteristics of duodenal gastrointestinal stromal tumors as predictors of malignancy. *World J Surg Onc.* 2013; 11.
15. Saturday GA, Lasota J, Frost D, Brasky KB, Hubbard G, Miettinen M: KIT-positive gastrointestinal stromal tumor in a 22-year-old male chimpanzee (*Pan troglodites*). *Vet Pathol*. 2005; 42: 362-365.
16. Ueda K, Takanosu M, Kagawa Y, et al. Gastrointestinal stromal tumors with *Kit* gene mutation in 4 guinea pigs (*Cavia porcellus*). *Vet Pathol*. 2022. 59(5): 740-746.
17. Yang DY, Wang X, Yuan WJ, Chen ZH: Metastatic pattern and prognosis of gastrointestinal stromal tumor (GIST): a SEER-based analysis. *Clin Transl Oncol*. 2019.